Scanning Electron Microscope In-Situ Investigation of Fracture Behavior in 96.5Sn3.5Ag Lead-Free Solder

YING DING,[1,3] CHUNQING WANG,[1] and MINGYU LI[2]

1.—Microjoining Laboratory, School of Materials Science and Engineering, Harbin Institute of Technology, Harbin 150001, People's Republic of China. 2.—Shenzhen Graduate School, Harbin Institute of Technology, Shenzhen 518055, People's Republic of China. 3.—E-mail: dyzoe@hit.edu.cn

In-situ tensile tests of as-cast 96.5Sn3.5Ag eutectic solder were performed under the scanning electron microscope (SEM) using different strain rates at room temperature, and various crack initiation and propagation behavior was observed on the specimen surface. It was found that, due to the existence of Ag_3Sn intermetallic particles and the special microstructure of β-Sn phases in Sn3.5Ag solder, grain boundary sliding (GBS) was no longer the dominant mechanism for this Pb-free solder. In the lower strain rate regime, accompanied by partial intragranular cracks, intergranular fracture along the grain boundaries in Sn-Ag eutectic structure or along the interphase boundaries between Sn-rich dendrites and Sn-Ag eutectic phases occurred primarily for the Sn3.5Ag solder in the early tensile stage. However, significant plastic deformation was observed in large areas for the specimens tested at higher strain rates, and cracks propagated in a transgranular manner across the Sn dendrites and Sn-Ag eutectic structure.

Key words: 96.5Sn3.5Ag eutectic solder, Ag_3Sn, in-situ scanning electron microscope (SEM), tensile rate, deformation behavior

INTRODUCTION

Pb-free solder alloys are intended to completely substitute for traditional solder materials containing Pb due to environmental and health concerns.[1] Sn-Ag eutectic solder is a promising candidate for this requirement because of its higher strength and superior resistance to creep and thermal fatigue, when compared to eutectic Pb-Sn solder.[2] Therefore, it is very important to understand the mechanical properties and fracture behavior of this alloy in order to allow improved prediction of the reliability of Pb-free solder joints in electronic packaging and assemblies. Research has been conducted in some areas, such as isothermal fatigue behavior, tensile properties, and microstructure change during creep.[3–11] Solomon[3] found that the fatigue resistance of 96.5Sn3.5Ag was superior to that of Sn-Pb eutectic solder for total shear-strain-controlled fatigue tests at 35°C and 150°C. Liang[4] reported that grain boundaries of tin-rich phases in 95Sn-5Ag eutectic alloy are weak spots for cracking during the low cycle fatigue tests. Igoshev[5] indicated that, depending on the applied stress and temperature, grain boundary (GB) cracking phenomena can affect the creep rate and, consequently, contribute to the calculated value of creep activation energy. Kanchanomai[8–10] found that steps at the boundaries of Sn dendrites were the initiation sites for microcracks in the case of low-frequency (10^{-3} Hz) fatigue tests, while for high-frequency (1 Hz) tests, cracks predominantly initiated at the boundaries of subgrains formed in Sn dendrites. Recently, Kerr studied the creep deformation behavior of Sn3.5Ag solder at small length scales,[11] and a change in the stress exponent with increasing stress was observed and explained in terms of a threshold stress for dislocation motion, due to the presence of obstacles in the form of Ag_3Sn particles. However, except for these countable reports on the mechanical behavior of Sn-Ag eutectic solder, little is known about the dynamic process of crack initiation and propagation

(Received March 15, 2005; accepted June 14, 2005)

Table I. Chemical Composition of 96.5Sn3.5Ag Solder (Wt.%)

Sn	Ag	Sb	Cu	Bi	As	Fe	Zn	Al
Bal.	3.484	0.063	0.03	0.014	0.005	0.002	0.0010	0.0009

in Sn3.5Ag alloy, which might be necessary to research the deformation mechanism of the solder more thoroughly.

The main purpose of the current work is to investigate the basic characteristics of the fracture behavior in Sn3.5Ag solder under different tensile rates, using in-situ scanning electron microscope (SEM) observation. The dynamic development of the damage was recorded, and the possible reasons were discussed in detail.

MATERIALS AND EXPERIMENTAL PROCEDURES

The Sn-Ag eutectic solder, which was supplied in as-solidified form, was used in the present study. Ingots of 99.9% Sn and 99.9% Ag were melted in air under temperature of 420°C and cast into a steel mold. The material then was left to cool by 50°Cs^{-1} in air. The chemical composition of the specimen is given in Table I. In order to reveal the microstructure, the solder was etched with etchant 2 g of $FeCl_3$, 5 mL of HCl, 30 mL of distilled water, and 50 mL of alcohol. Figure 1 shows the SEM micrograph of the Sn-Ag eutectic alloy. Under equilibrium conditions, the phase diagram of the Sn-Ag system at the eutectic composition predicts a microstructure consisting of a mixture of Ag_3Sn (ε) and Sn. However, the cooling rate of 50 °C s^{-1} for the current Sn3.5Ag solder resulted in non-equilibrium solidification, and yielded a microstructure of primary Sn (β)-rich dendrites (dark) surrounded by a fine eutectic mixture (light) of circular or needlelike Ag_3Sn in a Sn-rich matrix, as shown in the figure. Moreover, a relatively fast cooling rate also led to the obvious GB in eutectic structure, as indicated by the arrow in Fig. 1.

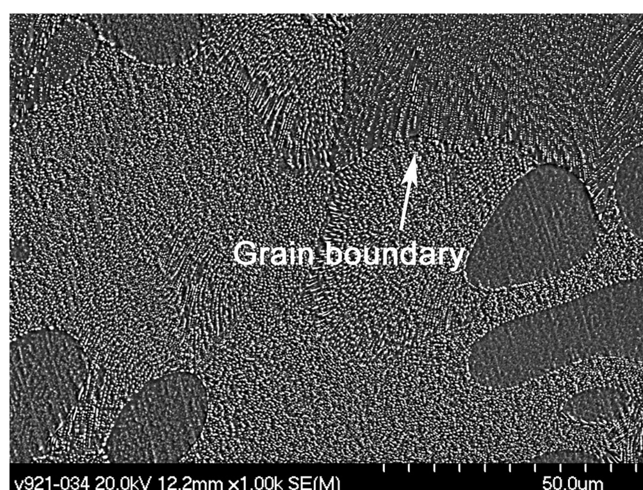

Fig. 1. SEM micrograph of Sn-Ag eutectic solder.

In order to quantify the relationship between the mechanical properties and strain rates, monotonic tensile tests were conducted by an Instron 5569 Electron Universal Material Testing Machine (Instron, U.K.) at 25 °C with three displacement rates—5 mm min^{-1}, 0.5 mm min^{-1}, and 0.05 mm min^{-1}. If using the strain rate as a standard, this equals about 5.6×10^{-3} s^{-1}, 5.6×10^{-4} s^{-1}, and 5.6×10^{-5} s^{-1}. Then, from bulk solder bar materials, the in-situ SEM specimens were machined on a linear cutting (LC) machine. The specimen, which was designed according to the operation demand of the SEM, has a flat dog bone shape (2.0-mm thick, 12-mm wide, 38-mm long; 5.0-mm wide and 6.0-mm long gage section). For observation convenience, a notch was made in the middle of the specimen side face with the LC machine, and its depth was approximately 1 mm. The in-situ tensile experiment was performed in a HITACHI S-570 SEM (Hitachi, Japan) with a maximal load capacity of 2 kN at ambient temperature. For Sn-Pb eutectic solder, the fracture mechanism changed from intergranular-dominated to transgranular-dominated when the strain rate was increased, and the critical value was 10^{-3} s^{-1}.[12] In this SEM in-situ study, two kinds of displacement rates ($\dot{L}$) were employed—0.05 mm min^{-1} and 1 mm min^{-1}—in order to be equivalent to approximately below 10^{-3} s^{-1}, and higher than the value in strain rate for the purpose of comparison with the previous work. During this procedure, the straining was stopped several times in order to make observations and take micrographs while the load was still applied.

RESULTS AND DISCUSSION

Mechanical Properties and Parameters of 96.5Sn3.5Ag Lead-Free Solder

After the monotonic tensile tests, the curves of axial stress-strain with different strain rates were achieved, as shown in Fig. 2. The strength and plasticity of Sn3.5Ag increased with increased rate. These phenomena differed from that of 63Sn37Pb solder, which exhibited superplasticity when the strain rate was low enough,[13] but poor plasticity with quick deformation. The resultant modulus of elasticity with the medial strain rate was 47 GPa, and the measured stress exponent, n, at room temperature was 11.6. If the creep was defined as power-law behavior, then the strain rate could be expressed as follows:

$$\dot{\varepsilon} = A\sigma^n = (A'\sigma)^n$$

Here, the constant A' in our study was approximately −1.5 that of the same A' value of 63Sn37Pb solder in Ref. 14. However, the stress exponent of

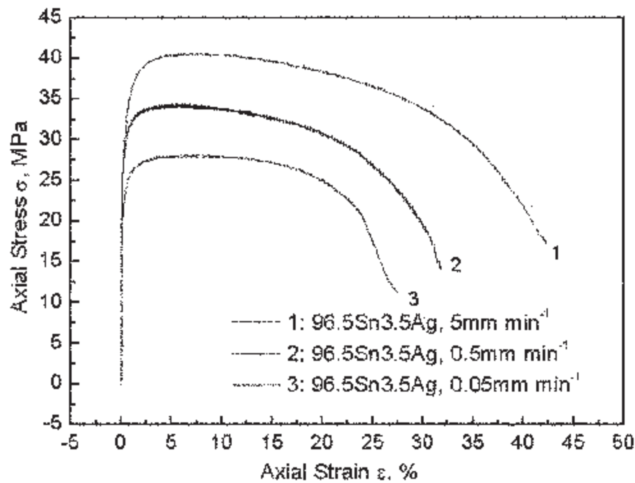

Fig. 2. Axial stress-strain curve of 96.5Sn3.5Ag eutectic solder for different displacement rates in monotonic loading.

the latter, ~7.2, was lower than the former in the same monotonic loading condition, which means that Sn3.5Ag has better creep resistance compared with the Sn-Pb eutectic.

Fracture Behavior and Mechanisms in the Low Tensile Rate Regime ($\dot{L} = 0.05$ mm min^{-1})

Through SEM in-situ tensile testing, the dynamic fracture behavior of 96.5Sn3.5Ag solder was recorded in real time. Macrodeformation process near the notch with lower displacement rate was shown in Fig. 3. It can be seen that the notch has been widened. Due to stress concentration, cracks originated in the vicinity of the notch (areas A and B), and grew in size with increased loading. Accompanied by the slip behavior to a certain degree in the later tensile stage, obvious plastic deformation occurred along the maximum shear stress direction.

Figure 4 showed the specific evolution of area A in Fig. 3. It was found that, in the early stage, microcracks initiated along the grain boundaries (CD, EF) in eutectic structure, and along the interphase boundaries (FGH) between Sn dendrites and Sn-Ag eutectic phases. The crack along the boundary EF continued to propagate, and then a cavity was formed here. Later, further GB behavior was constrained. More slip bands along the maximum shear stress direction (45° angle to the loading direction) presented at the specimen surface. In the straining concentration area, grains were prolonged along the loading direction, such as Sn dendrites O and P in Fig. 4b. Then, drastic deformation was centralized within these grains, and transgranular cracks appeared, as shown in Fig. 4c. Finally, the cavity along the boundary EF did not develop, and the main crack was generated and propagated through grain O, P, and R (Fig. 4d). During this process, separate small cavities were sometimes also observed along the grain or phase boundaries, as shown in Fig. 4b. However, with the coming remarkable plastic deformation and the development of the main crack, they did not coalesce and propagate at later stage.

It was reported that the creep behavior of Sn-rich solders is dominated by the behavior of Sn matrix.[15] Therefore, at high homologous temperature (~0.60 T/T_m at room temperature for Sn3.5Ag), the deformation in Sn-Ag eutectic solder was ready to follow the grain boundary sliding (GBS) mechanism that was dominant during the deformation process of the pure tin.[16] Moreover, both the grain boundaries in the eutectic structure and the interphase boundaries between Sn dendrites and Sn-Ag eutectic phases can be considered as weak areas. These areas have high free-energy, stress concentration, and diffusion processes, and boundary sliding might occur. However, the second-phase particles of Ag_3Sn, which existed along the grain boundaries (GBs) in eutectic and the boundaries of Sn dendrites, obstructed and reduced the boundary sliding. More importantly, the 96.5Sn3.5Ag solder has a special

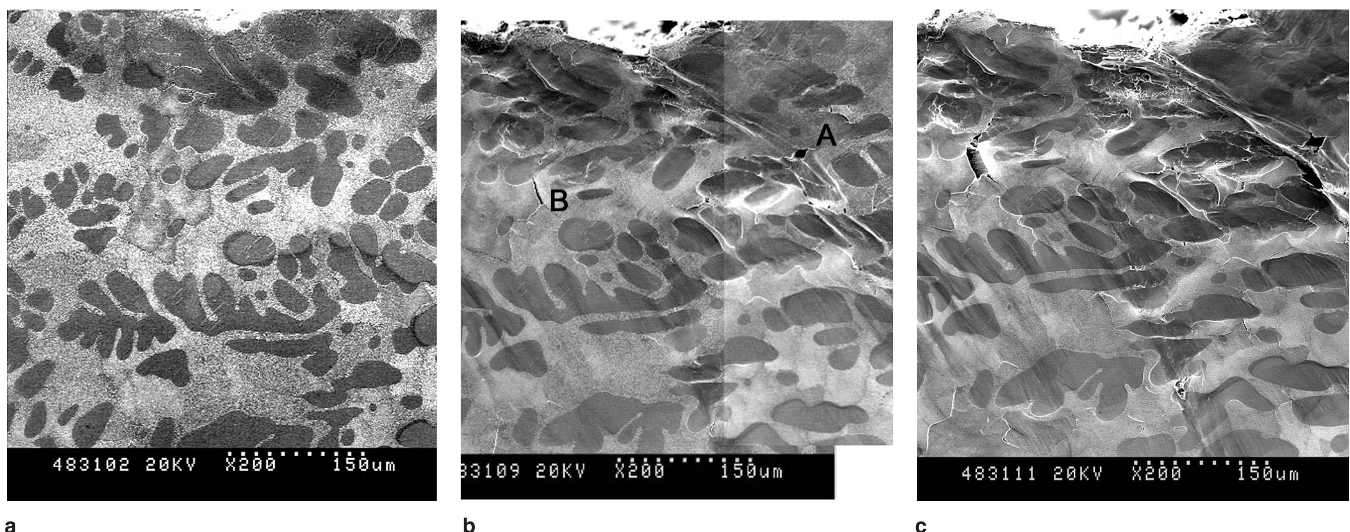

Fig. 3. Macrodeformation process near the notch of Sn3.5Ag specimen strained to (a) 1.1%, (b) 4.6%, and (c) 5.9% at 298 K (strain rate $< 10^{-3}$ s^{-1}, load direction in horizontal).

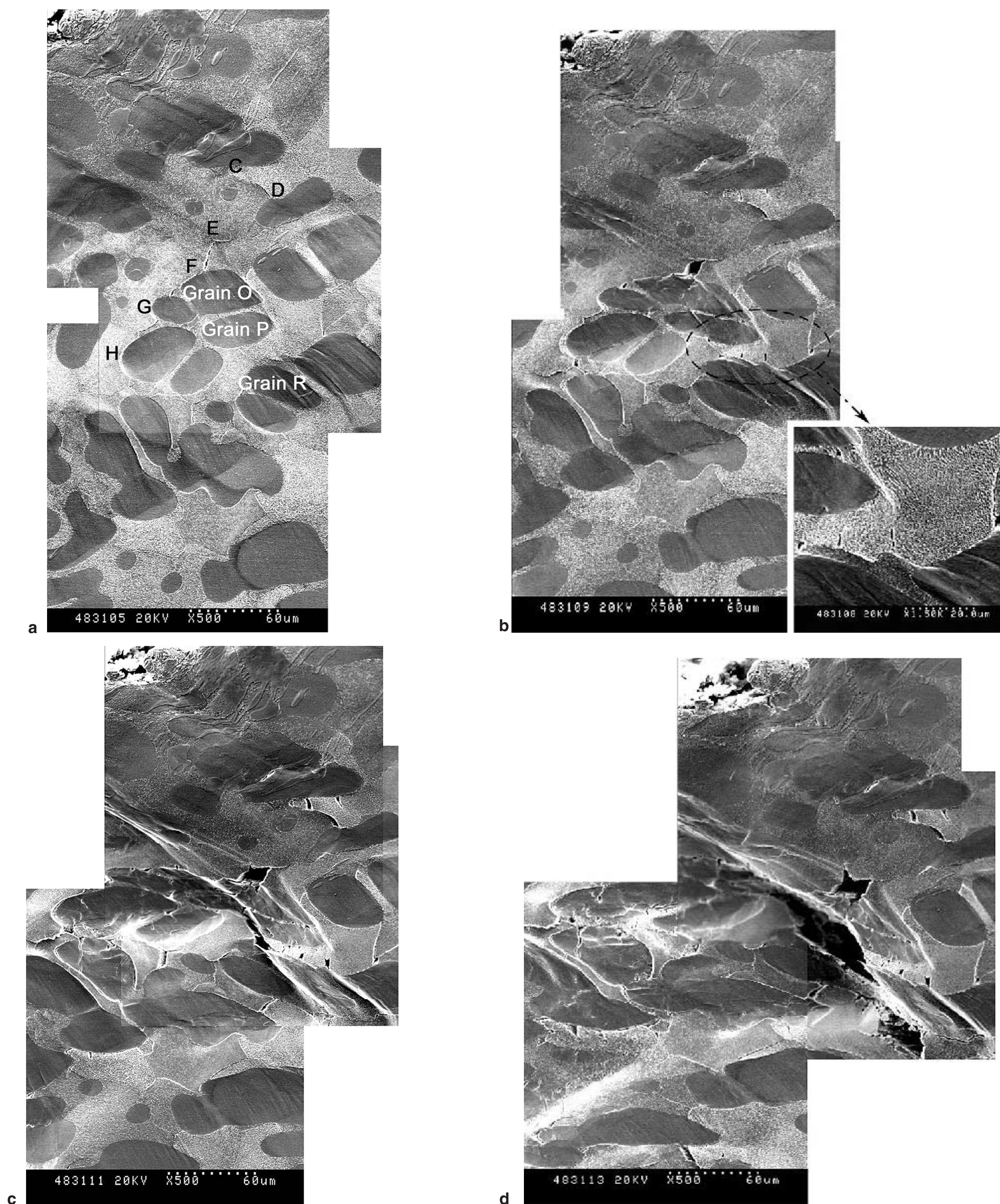

Fig. 4. Damage evolution in area A in Fig. 3 with high magnification strained to (a) 3.8%, (b) 5.0%, (c) 5.7%, and (d) 6.5% at 298 K (strain rate $< 10^{-3}$ s^{-1}, load direction in horizontal).

microstructure—primary Sn-rich dendrites. The nature of dendrite structure, similar to the branches of a tree, is not favorable for the sliding process along GBs.[9] Thus, it is not surprising that the sliding process is not the dominant mechanism for this Pb-free solder as it was in the case of the 63Sn37Pb solder.[17] The presence of particles of hard intermetallic inclusions at GBs in the Sn3.5Ag alloy did not allow for the process of stress concentration relaxation by GBS mechanism. Then let us assume

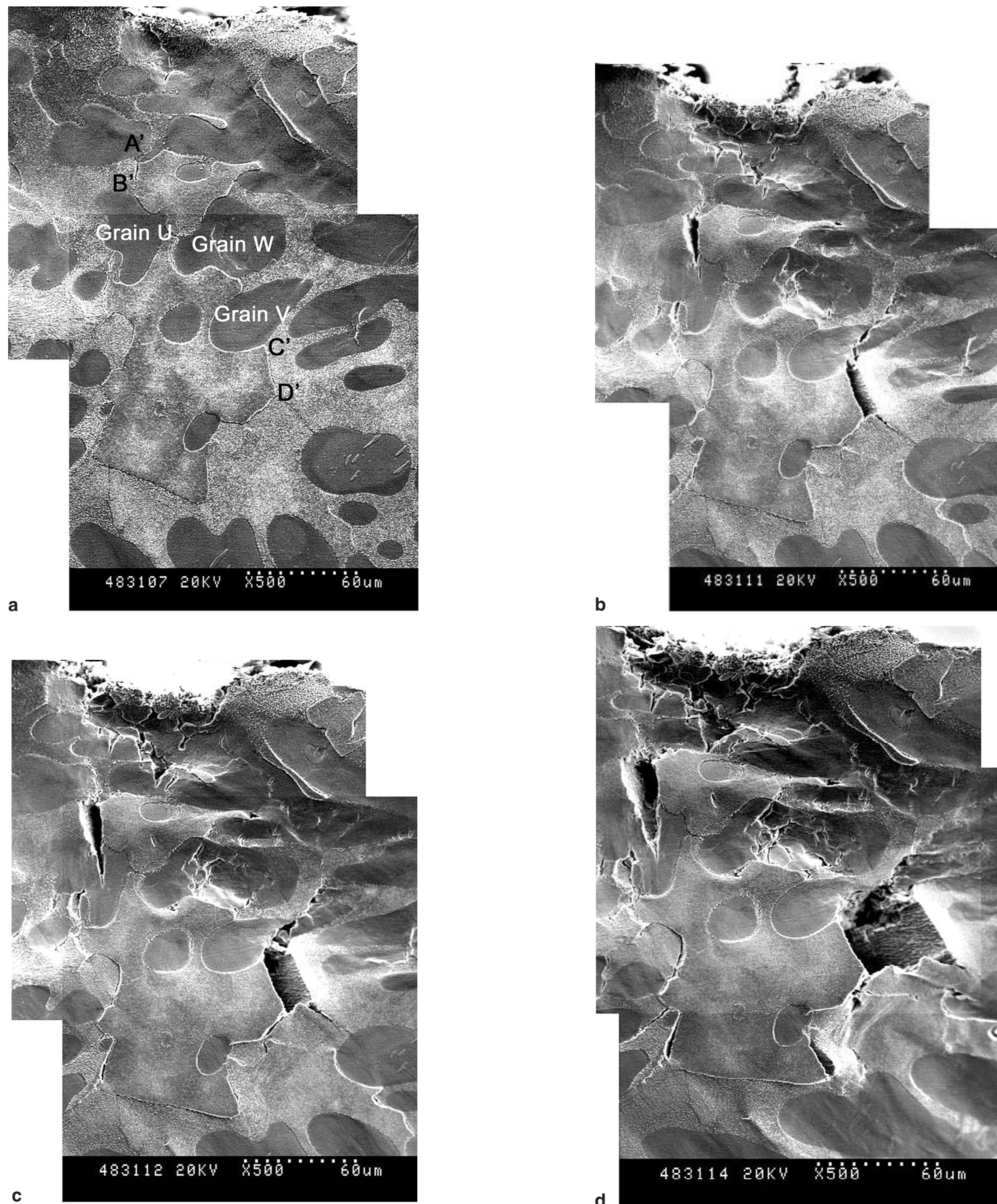

Fig. 5. Surface configuration of area B in Fig. 3 during tensile process with high magnification strained to (a) 4.8%, (b) 5.7%, (c) 5.9%, and (d) 7.4% at 298 K (strain rate $< 10^{-3}$ s^{-1}, load direction in horizontal).

that, due to such stress concentration along GB, a failure (microcrack or void nucleation) appears around the small particle of the GB's intermetallics. Once created, such a defect serves as a vacancy sink in the process of stress relaxation. It grows by diffusive mass transport along GBs. The driving force of this kinetic process is the local stress concentration sustained by the creep deformation of the specimen within a small strain range. As the defect grows, the GB displacement becomes possible which, in turn, leads to the formation of a boundary crack on the surface.

Figure 5 shows the surface morphology during the tensile process in another area with severe fracture in Fig. 3, area B. Obviously, cracks originated and expanded along the grain boundaries in Sn-Ag eutectic structure, especially along the boundary A'B' and C'D'. On the other hand, due to the limitation of intensive boundary behavior, intragranular rupture also occurred in some sites to relax the

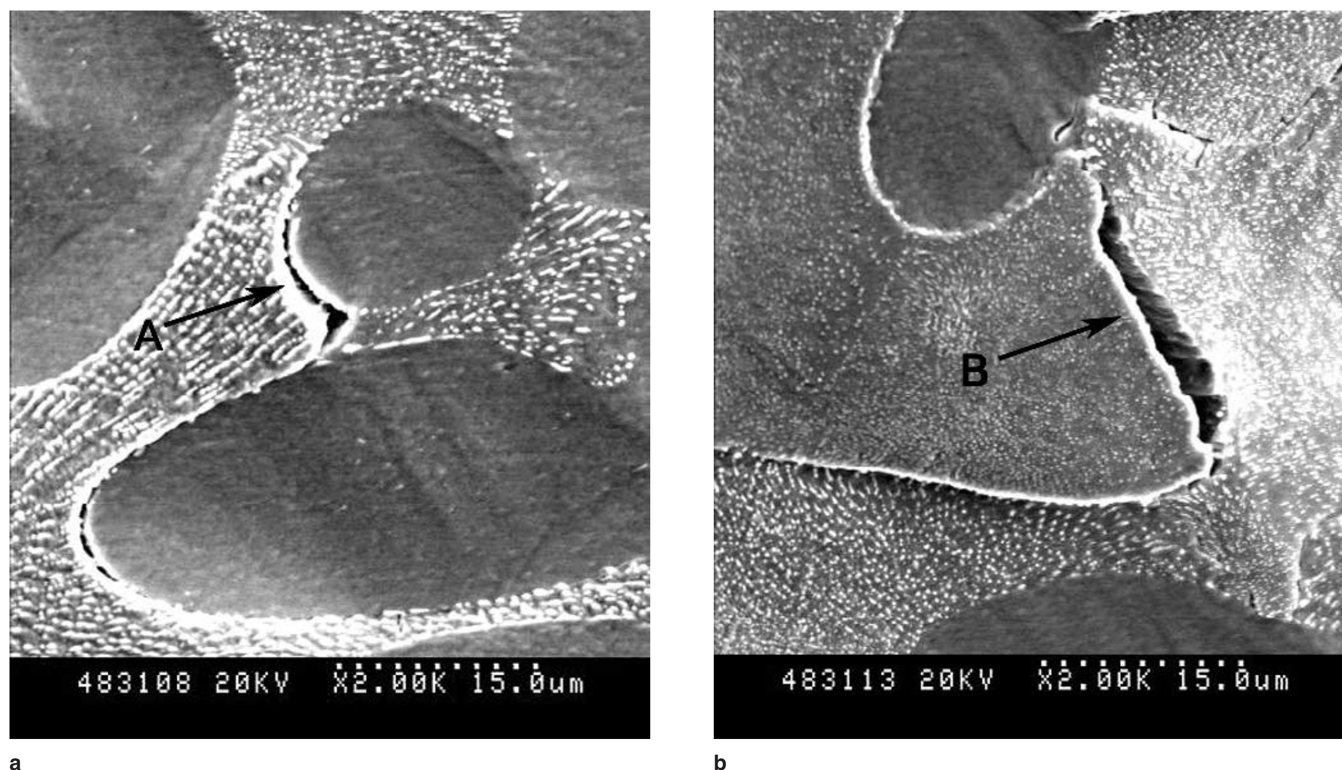

a b

Fig. 6. The SEM micrographs of local surface configuration in the Sn3.5Ag specimen strained to 3.9% at 298 K, showing intergranular cracks along (a) the Sn-dendrite boundary (arrow A) and (b) the boundary in eutectic structure (arrow B) (strain rate $< 10^{-3}$ s^{-1}, load direction in horizontal).

surplus stress concentration, like grain W in the figure. With increasing loading time, multiple transgranular cracks were detected near the notch. Intergranular cracks initiated along the boundary A'B' and C'D' were finally propagated through the grain U and V, respectively, as shown in Fig. 4d. Thus, in the early tensile stage, the formations of intergranular cracks were isolated and independent. On further straining, under the influence of the special structure of Sn-rich dendrites, these cracks were controlled to some extent in sizes and depths. After a period of loading, some of these cracks eventually attempted to link-up to form larger cracks, resulting in the emergence of both intergranular crack and transgranular crack.

Local deformation behavior was also traced to further understand the fracture mechanism of Sn3.5Ag specimen at low displacement rate. Examples of local intergranular cracks either along Sn dendrites boundary or along grain boundaries in the eutectic structure were indicated by arrows in Fig. 6 with high magnification. At the same time, transgranular cracks were also observed distinctly, by cutting through either the Sn-Ag eutectic structure or the Sn-rich dendrites, as shown in Fig. 7. Moreover, the Ag_3Sn particles have a higher stiffness(E_{Ag3Sn} $\sim$ 80 GPa) than the surrounding Sn-rich phases (E_{Sn} $\sim$ 46 GPa), and the deformation resistance of Ag_3Sn is naturally much higher than that of the β-Sn matrix. Therefore, because of the difference in deformation between both regions, interphase cracks might appear. Conversely, since the Sn matrix was softer than the eutectic, most of the stress and strain take place in the dendrites, which results in heavier intragranular fracture of the Sn dendrites, as shown in Fig. 7.

Figure 8 shows the surface deformation configuration of the area containing rod-shaped Ag_3Sn in the specimen tested at low tensile rate. It should be noted that the fine and uniform dispersion of Ag_3Sn will enhance the strength of the alloy by providing more efficient obstacles for dislocation motion. Also, they will supply the nucleation source and activate the formation of intergranular defects within a small strain range. While the large Ag_3Sn eutectic rods only cause some surface microcracks engendered around them (as can be seen in Fig. 8), these microcracks did not differ greatly afterward.

Above all, due to the existence of fine particles Ag_3Sn in Sn3.5Ag solder and the special microstructure of Sn dendrites, boundary behavior was limited. However, high homologous temperature, together with lower deformation rate, caused Sn3.5Ag eutectic solder to exhibit creep behavior to some extent. Under this condition, along with partial transgranular cracks, intergranular fracture was the dominant mechanism in the early tensile stage.

Fracture Behavior and Mechanisms in the High Tensile Rate Regime ($\dot{L} = 1$ mm min^{-1})

In a higher loading rate regime, GB behavior could not keep up with the tensile rate. This means that the contribution from boundary behavior could not be expected to relax the quickly increased stress

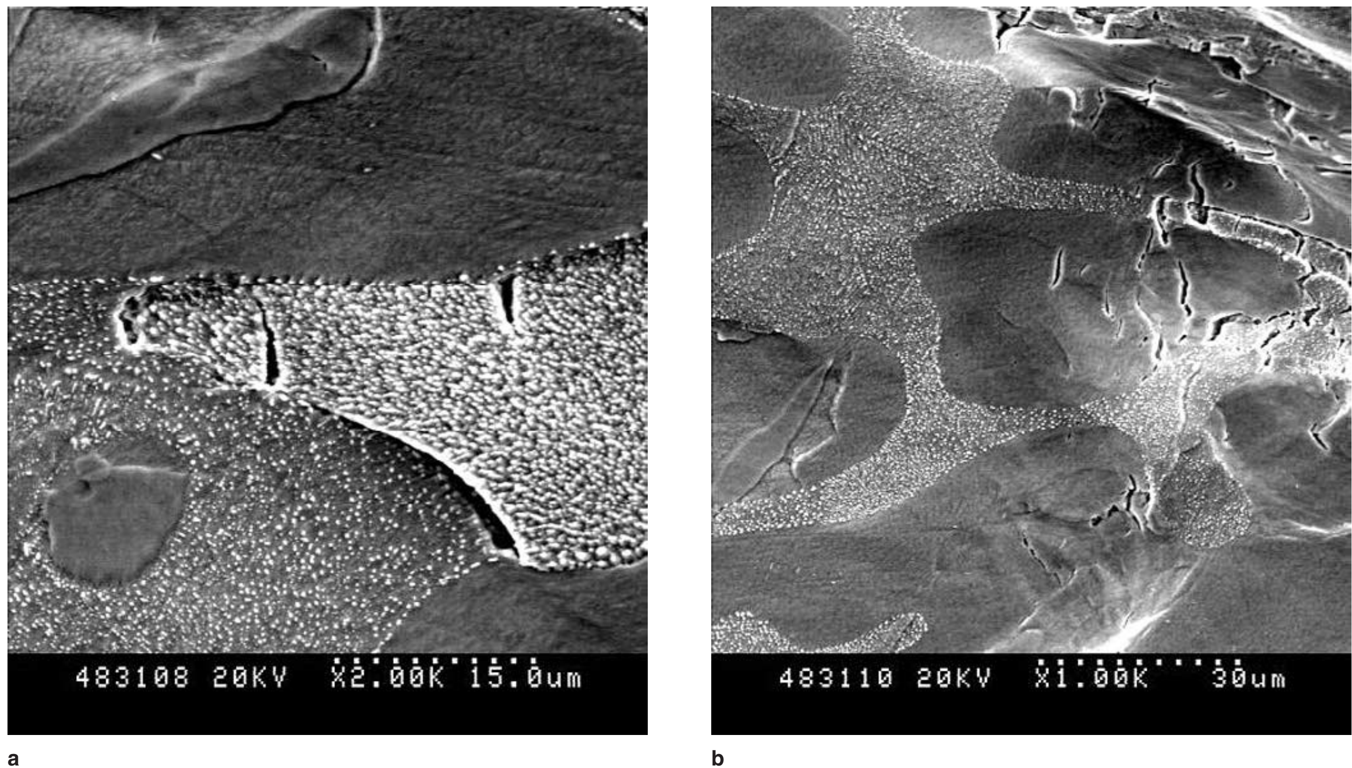

Fig. 7. The SEM micrographs of local surface configuration in the Sn3.5Ag specimen strained to 5.4% at 298 K, showing transgranular cracks through (a) Sn-Ag eutectic structure and (b) the Sn-rich dendrites (strain rate $< 10^{-3}$ s^{-1}, load direction in horizontal).

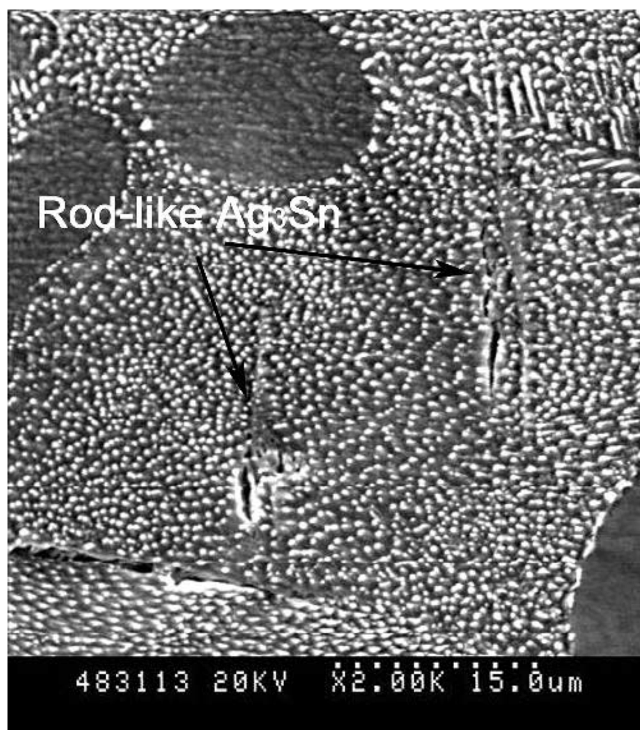

Fig. 8. The SEM micrograph of local surface configuration in the area containing rodlike Ag_3Sn in the Sn3.5Ag specimen strained to 6.5% at 298 K (strain rate $< 10^{-3}$ s^{-1}, load direction in horizontal).

concentration in time. Figure 9 shows the macrodeformation process near the notch with higher displacement rate. Plastic flow was notable, even in the early tensile stage, and the specimen surface turned white under the influence of slip bands everywhere. No obvious macrocrack was visible. It is reasonable to suggest that many dislocations were activated within grains, and the dislocation density was increased. Mobile dislocations were pinned by the fine Ag_3Sn particles, which strengthened the solder alloys more efficiently in this condition. Combined with the relevant mechanical properties, the strength in this case was higher. This agrees well with the Taylor yielding strength theory:[18]

$$\tau_y = \alpha G b \sqrt{\rho}$$

where b is Burgers vector modulus, ρ is dislocation density, α is a geometric constant, and G is shear modulus. At the same time, plastic deformation evolved fully due to the constraining of serious intergranular cracks, which also increased the strain to failure.

In order to observe the microdeformation process, the variation of surface morphology in area C in Fig. 9 was inspected, as shown in Fig. 10. It was noted that grains were distorted soon with the fast straining. The boundaries of interphase were unclear under the influence of considerable plastic flow. Positions O and P were further traced with high magnification to understand the boundary behavior in the case of higher strain rate. Figure 11 shows the deformation phenomena in position O. It was found that the intergranular microcrack initially nucleated at the Sn-dendrite boundary E'F' and did not propagate before the serious intragranular cracks appeared, like grain

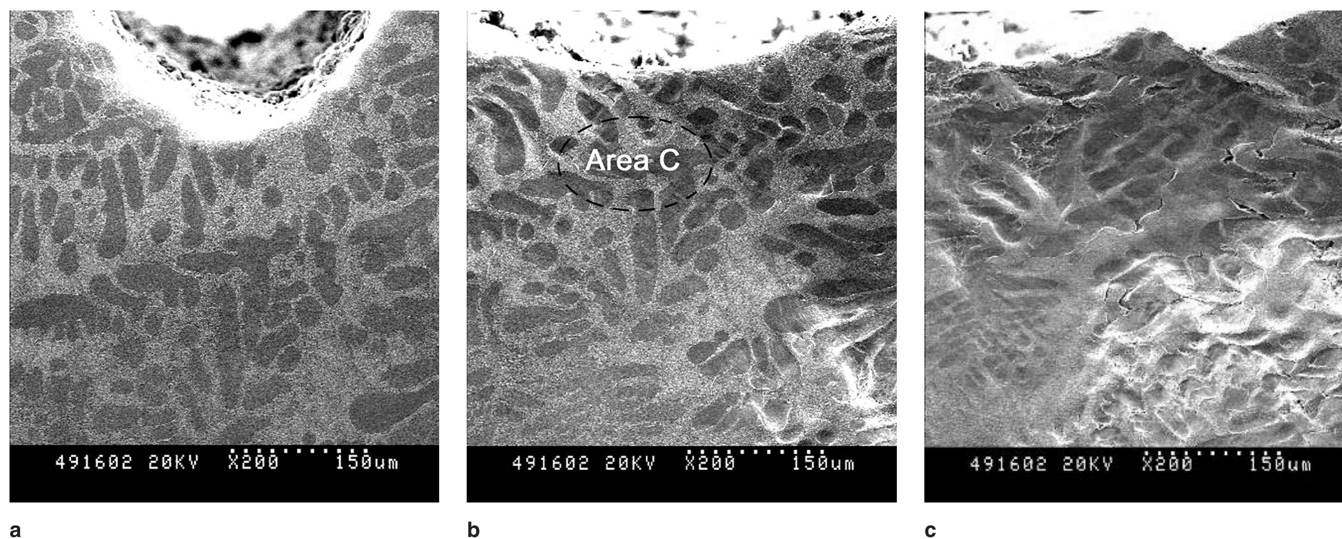

Fig. 9. Macrodeformation process near the notch of Sn3.5Ag specimen strained to (a) 0%, (b) 4.2%, and (c) 7.3% at 298 K (strain rate $> 10^{-3}$ s^{-1}, load direction in horizontal).

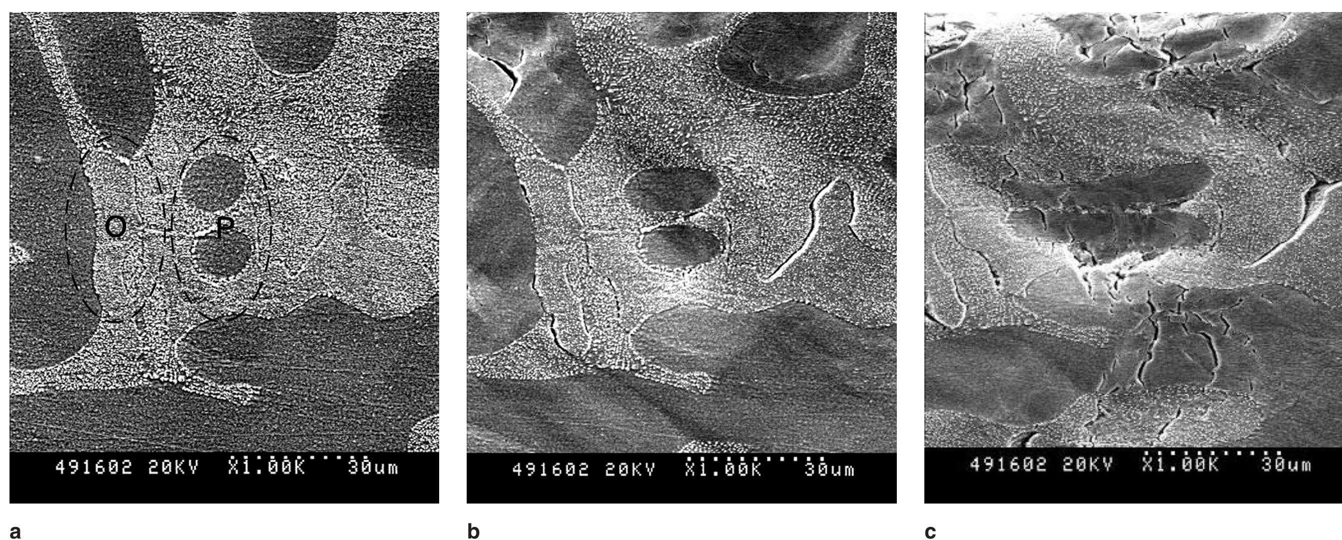

Fig. 10. Microdeformation process in area C under the notch in Fig. 9, strained to (a) 0%, (b) 4.2%, and (c) 6.1% at 298 K (strain rate $> 10^{-3}$ s^{-1}, load direction in horizontal).

N. It is the same for position P, as can be seen in Fig. 12. Microcracks attempted to originate along the boundaries IJK and LM in the Sn-Ag eutectic structure at first, but later the transgranular fracture was entirely dominant during the fast deformation process. It should be noted that, when drastic transgranular cracks were obstructed by the small Ag_3Sn particles, the latter were drawn apart from the matrix under the power of the stress. Here, some separated particles of second phase can be detected in Fig. 12d.

Examination of local deformation behavior in the Sn3.5Ag solder revealed that obvious intragranular deformation has sometimes been carried out before the nucleation of the boundary cracks under the higher strain rate. Evidence can be provided in Fig. 13 by the appearance of slip lines and the microcracks within the grain. Furthermore, the stress concentration in the Sn-rich dendrites (which have lower strength and stiffness than the Sn-Ag eutectic) will cause the intragranular fracture more easily here. The failure mode, therefore, has close relations with the configurations of the dendrite microstructure. Figure 14 indicates that different deformation results can be produced with different dendritic morphology in the same deforming region of the specimen. Serious intragranular cracks were preferable in the large Sn dendrite, as shown in Fig. 14a. On the contrary, when the Sn dendrites were relatively small, intergranular cracks along the interphase boundaries between Sn-Ag eutectic structure and the Sn-rich phase evolved more sufficiently than the former (Fig. 14b).

Due to the higher strain rate, the boundary behavior presented in the initial stage was quickly substituted by the intragranular deformation and

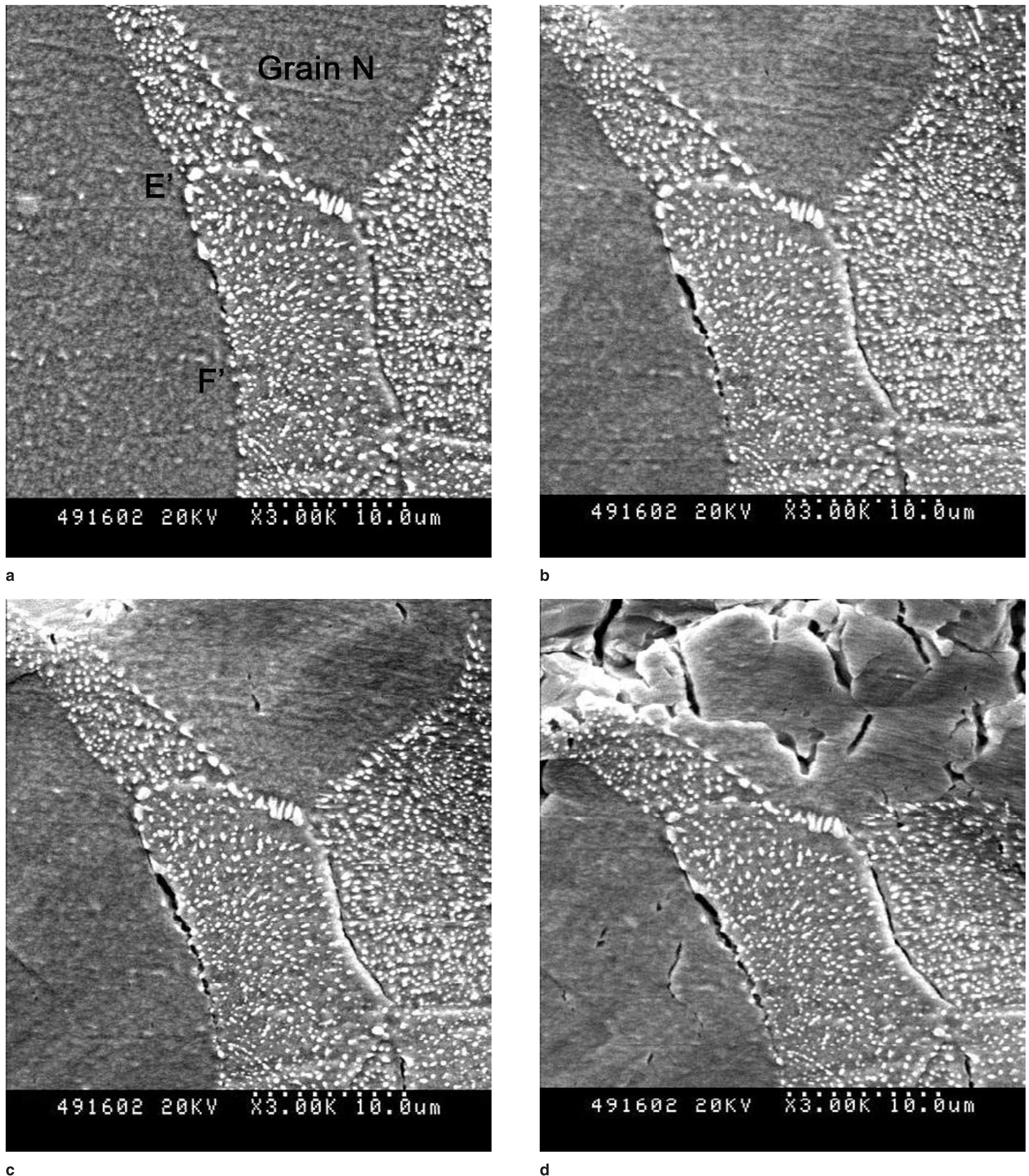

Fig. 11. Deformation phenomena in position O in Fig. 10 with high magnification, strained to (a) 1.2%, (b) 4.2%, (c) 5.0%, and (d) 6.1% at 298 K (strain rate $> 10^{-3}$ s^{-1}, load direction in horizontal).

fracture before it could grow further. The elevation of the tensile rate constrained the intergranular fracture, but promoted the development of cracks intragranularly.

A comparison between the mechanical properties of the Sn3.5Ag studied here, to previous research on 63Sn37Pb solders,[17] indicates that both solders exhibited different deformation behavior under the

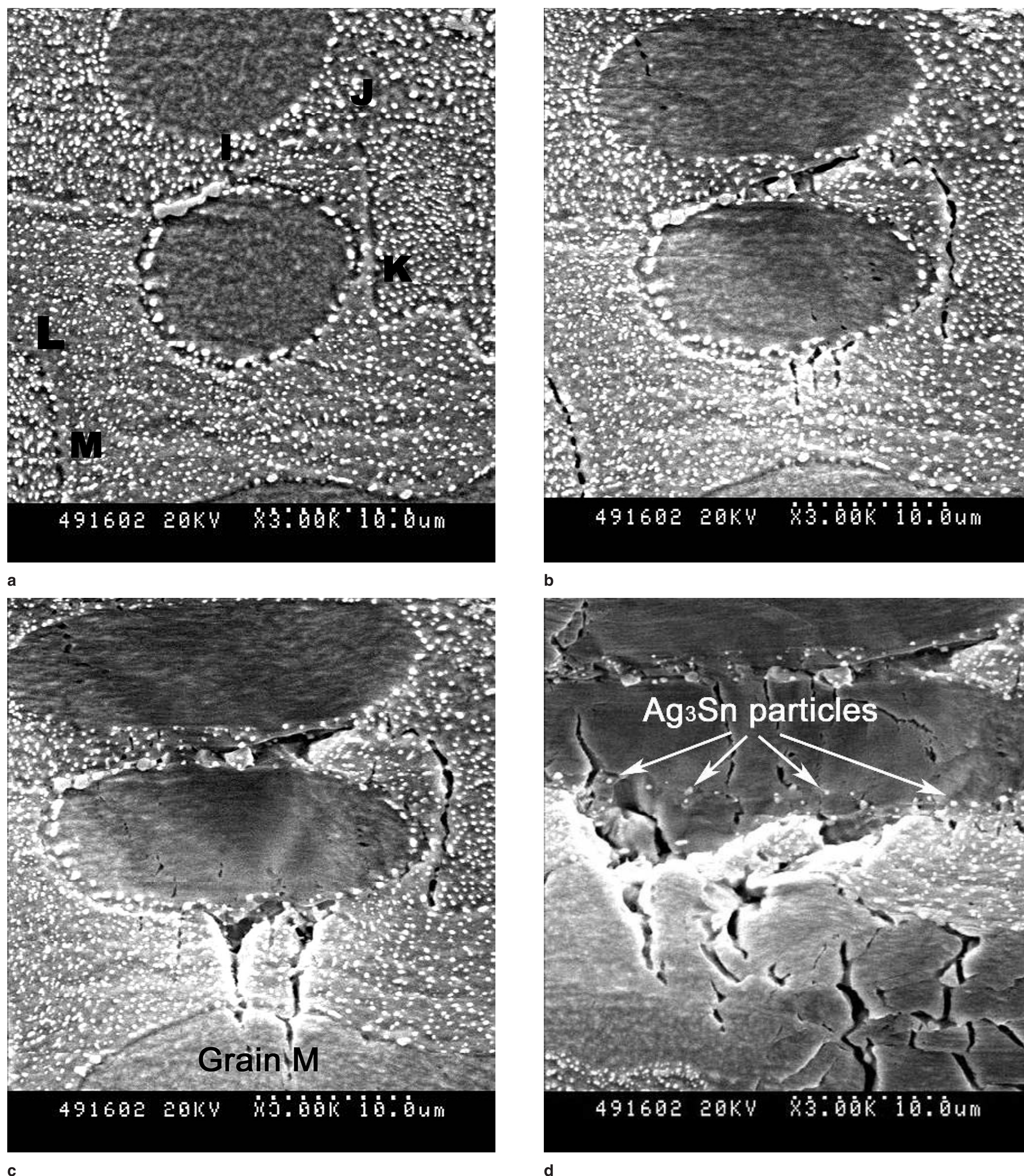

Fig. 12. Deformation phenomena in position P in Fig. 10 with high magnification, strained to (a) 1.2%, (b) 4.2%, (c) 5.0%, and (d) 6.1% at 298 K (strain rate $> 10^{-3}$ s^{-1}, load direction in horizontal).

same loading condition. For Sn-Pb eutectic alloy, Sn and Pb are all the IV main group elements in the periodic table, and the fifth and sixth periodicity, respectively. The arranging positions are closely distributed, and they are compatible. There are not intermetallic products. In contrast, for Sn-Ag eutectic, Ag is the transition group element in the fifth periodicity and reacts drastically with Sn, forming intermetallic Ag_3Sn. Mobile dislocations are arrested and slowed at these particles, which strengthens

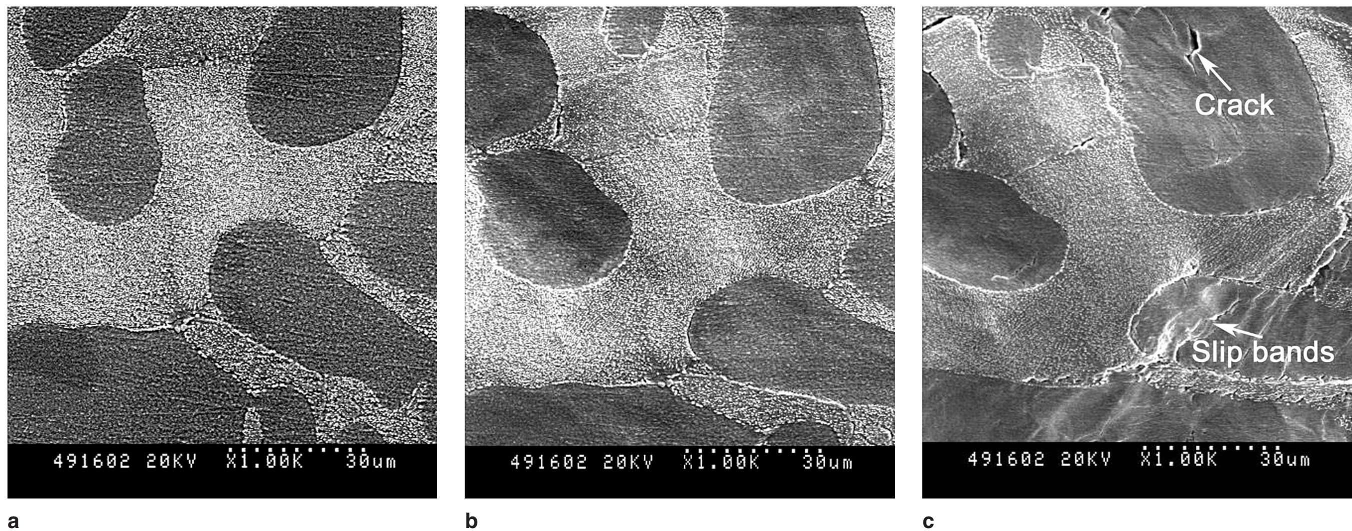

Fig. 13. Local deformation behavior of the specimen surface far away from the notch, strained to (a) 0%, (b) 4.2%, and (c) 7.3% at 298 K (strain rate $> 10^{-3}$ s^{-1}, load direction in horizontal).

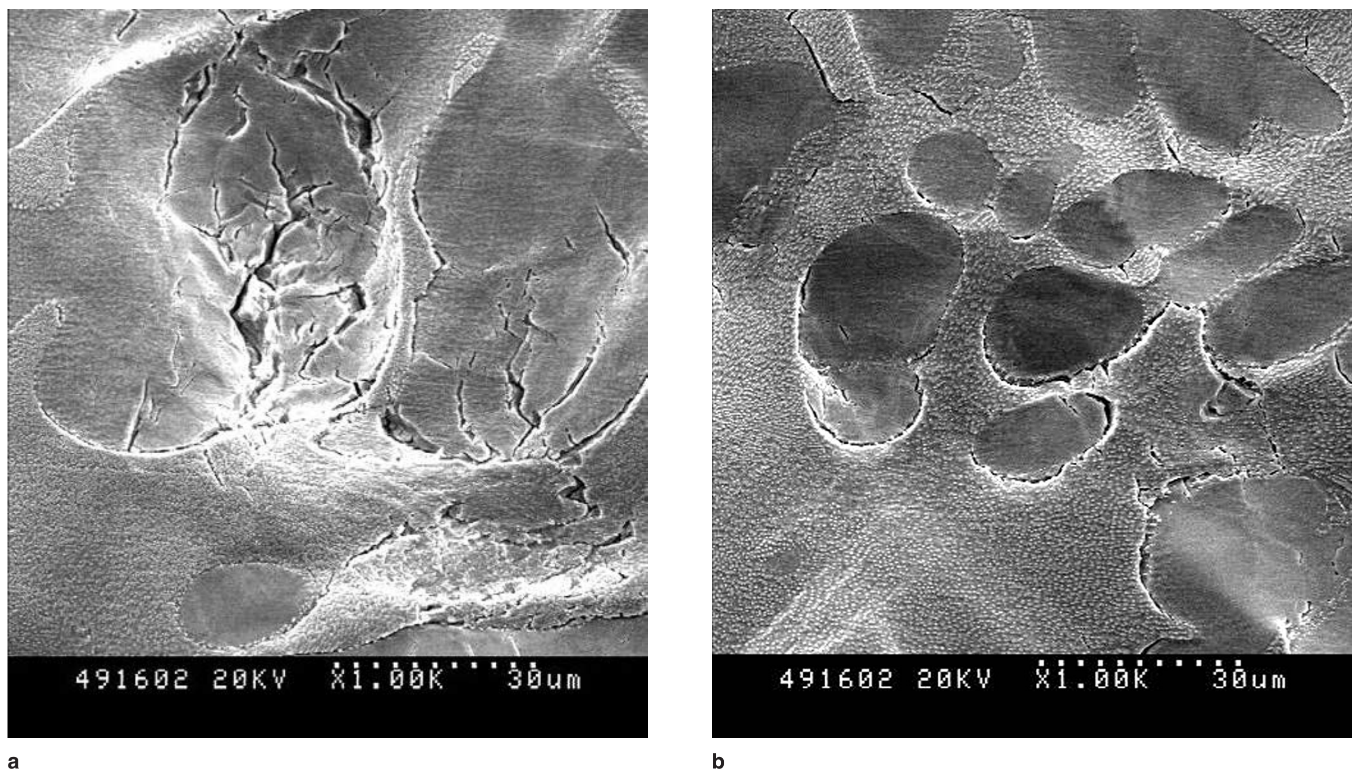

Fig. 14. A contrast of deformation results with (a) large and (b) small Sn-rich dendrites strained to 5.0% at 298 K (strain rate $> 10^{-3}$ s^{-1}, load direction in horizontal).

the solder remarkably. Simultaneously, the formation of Ag_3Sn particles comparted the small Sn particles in matrix. The finer the Ag_3Sn particles, the more effectively the compartmentation performs. The existence of these small particles restrained the fluidity and diffusibility of Sn atoms, which obstructs the boundary behavior to a certain extent since more vacancies are produced in the Sn matrix. In summary, two important differences exist between the solders. First, the Pb content in Sn-Pb eutectic is great, and the eutectic is a solid solution. Grain boundaries are rounded off, and the atom diffusion resistance is small, resulting in a GBS-dominated deformation mechanism. In Sn-Ag eutectic, the solid solubility of small amounts of Ag in the Sn matrix could be neglected, and all of the Ag in solution is almost turned to Ag_3Sn. The normal as-cast solidification rate could not get to the equilibrium station, and the structure of the primary precipitated Sn dendrites means that GBS is no longer the dominant mechanism. Second, the Ag_3Sn particles have a higher stiffness and strength than

the surrounding matrix. They strengthen the materials, but sacrifice the plasticity. However, Pb is known to be less stiff and weaker than the matrix. The strength is relatively lower, and toughness is better than the Sn-Ag eutectic.

CONCLUSIONS

Combining the mechanical properties testing and in-situ observation results, conclusions can be drawn for the deformation behavior of 96.5Sn3.5Ag solder alloys. It should be emphasized that microstructure is one of the key factors that influence the mechanical properties of the materials. The high solidification rate obtained with air cooling in this paper promoted nucleation but suppressed the growth of Ag_3Sn, yielding fine Ag_3Sn particles with spherical morphology dispersed in the Sn matrix. Affected by both the structure of Sn-rich dendrites and the encumbrance of Ag_3Sn particles, GBS was no longer the dominant deformation mechanism. In the lower strain rate, the creep property of Sn matrix was exerted, and the defects were accumulated around the second-phase particles by the diffusion process. Consequently, intergranular-dominated fracture occurred, especially in the early stage. In the higher strain rate, boundary behavior was limited under the fast straining, and plastic deformation and intragranular cracks appeared mainly during this procedure.

ACKNOWLEDGEMENT

The authors express their sincere thanks to the Ministry of National Space, the Second Research Institute, for supplying the solder ingots.

REFERENCES

1. F. Hua and J. Glazer, *Design and Reliability of Solder Interconnections*, ed. R.K. Mahidhara, D.R. Frear, S.M.L. Sastry, K.L. Murty, P.K. Liaw, and W. Winterbottom (Warrendale, PA: TMS, 1997), pp. 65–73.
2. W. Yang, L.E. Felton, and R.W. Messler, *J. Electron. Mater.* 24, 1465 (1995).
3. H.D. Solomon, *J. Electron. Packaging* 113, 102 (1991).
4. J. Liang, N. Gollhardt, P.S. Lee, S.A. Schroeder, and W.L. Morris, *Fatigue Fract. Eng. Mater. Struct.* 19, 1401 (1996).
5. V.I. Igoshev, J.I. Kleiman, D. Shangguan, C. Lock, S. Wong, and M. Wiseman, *J. Electron. Mater.* 27, 1367 (1998).
6. W.K. Jones, Y. Liu, M. Shah, and R. Clarke, *Soldering Surface Mount Technol.* 10, 37 (1998).
7. Y. Karita, Y. Hirata, and M. Otsuka, *J. Electron. Mater.* 28, 1263 (1999).
8. C. Kanchanomai, Y. Miyashita, and Y. Mutoh, *J. Electron. Mater.* 31, 142 (2002).
9. C. Kanchanomai, Y. Miyashita, Y. Mutoh, and S.L. Mannan, *Mater. Sci. Eng. A* 345, 90 (2003).
10. C. Kanchanomai and Y. Mutoh, *Mater. Sci. Eng. A* 381, 113 (2004).
11. M. Kerr and N. Chawla, *JOM*, 56 (6) (2004), pp. 50–54.
12. C. Kanchanomai, Y. Miyashita, and Y. Mutoh, *Int. J. Fatigue* 24, 987 (2002).
13. S. Wiese, F. Feustel, and E. Meusel, *Sensors Actuators A* 99, 188 (2002).
14. Z. Guo, A.F. Sprecher, and H. Conrad, *J. Electron. Packaging* 114, 112 (1992).
15. J.W. Morris, Jr., H.G. Song, and F. Hua, *2003 Electron. Components Technol. Conf.,* 54 (2003).
16. Y. Ding, C.Q. Wang, M.Y. Li, and H. Bang, *Mater. Lett.* 59, 697 (2005).
17. Y. Ding, C. Wang, M. Li, and H.-S. Bang, *Mater. Sci. Eng. A* 384, 314 (2004).
18. Hael Mughrabi-Weinheim, *Materials Science and Technology: A Comprehensive Treatment* (New York: Cambridge, 1998), pp. 7–11.